International Journal of Computational Methods
Vol. 14, No. 2 (2017) 1750046 (15 pages)

DOI: 10.1142/S0219876217500463



# A SPH Implementation with Ignition and Growth and Afterburning Models for Aluminized Explosives

Guangyu Wang*,‡, Guirong Liu*, Qing Peng† and Suvranu De†

*Department of Aerospace Engineering and Engineering Mechanics
University of Cincinnati, Cincinnati, OH 45221-0070, USA

†Department of Mechanical, Aerospace and Nuclear Engineering
Rensselaer Polytechnic Institute Troy, NY 12180, USA
‡wangg3@mail.uc.edu

Received 22 April 2016
Accepted 27 September 2016
Published 1 November 2016

Aluminized explosives have been applied in military industry since decades ago. Compared with ideal explosives such as TNT, HMX, RDX, aluminized explosives feature both fast detonation and slow metal combustion chemistry, generating a complex multiphase reactive flow. Though aluminized explosives have been employed for a long time, the mechanism underneath the chemical process is still not thoroughly understood. In this paper, a smooth particle hydrodynamics (SPH) method incorporated ignition and growth model, and afterburning model has been proposed for the simulation of aluminized explosive. Ignition and growth model is currently the most popular model for the simulation of high explosives, which is capable of accurately reproducing arrival time of detonation front and pressure history of high explosives. It has been integrated in commercial software such as ANSYS-LS DYNA. In addition, an afterburning model has been integrated in the SPH code to simulate the combustion of aluminum particles. Simulation is compared with experiment and good agreement is observed. The proposed mathematical model can be used to study the detonation of aluminized explosives.

*Keywords*: Aluminized explosives; smooth particle hydrodynamics; ignition and growth model; afterburning model; numerical modeling of detonation.



## 1. Introduction

Aluminized explosives are high explosives using micrometer-scale (for example, 5–10 $\mu$m) aluminum particles as additive. The mass fraction of aluminum in aluminized explosives ranges from 20% to 40% or even higher. Different from ideal explosives like TNT, HMX, RDX, TATB, aluminized explosives feature both fast detonation and slow metal combustion. The detonation of high explosives happens in microseconds, however, the combustion of aluminum particles generally takes

‡Corresponding author.

milliseconds or even longer. Due to the addition of aluminum particles, aluminized explosives have relatively low brisance but high blast potential [Cook *et al.* (1957)].

The detonation of high explosives and combustion of aluminum particles are rather complicated phenomenon. The mechanism underneath the chemical process is still not thoroughly understood till today. Modeling detonation and subsequent combustion requires a detailed knowledge of the chemical kinetics [see Cooper and Kurowski (1996); Cooper (1996)]. Abundant research has been conducted on the topics, experimentally and numerically. Wilkins, Squier obtained the Chapman–Jouguet pressure and equation of state (EoS) of PBX 9404 through experiments [see Wilkins *et al.* (1965)]. Wackerle [1978] investigated the pressure history of PBX 9404 through planar shock initiation. Cook *et al.* [1957] measured detonation pressure and detonation velocity of TNT–Al and other aluminized explosives. Due to the complexity of the phenomenon, it takes longer time for researchers to understand the mechanism theoretically.

Bdzil *et al.* [2002] proposed detonation shock theory (DSD), which assumes that the velocity of detonation normal to the shock is solely a function of shock curvature. The theory has been integrated in their codes to study ANFO. Lee and Tarver [1980], Tarver and Hallquist [1981] proposed a mathematical model to study shock initiation of heterogeneous explosives. In the model, they first introduced the concept of ignition and growth. The model assumes pressure equilibrium between solid explosive and gaseous products. Afterwards, the model has been improved continuously. In addition to pressure equilibrium, Tarver and McGuire [2002] further introduced temperature equilibrium as closure condition in their model. After that, ignition and growth model has been applied to study various high explosives, such as TATB, LX-17 and polymer-bonded explosives PBX 9404, PBX 9501 [Tarver (2005); Tarver and Chidester (2009); Tarver *et al.* (2002)]. Compared with Jones–Wilkins–Lee (JWL)++ model [Souers *et al.* (2000)], ignition and growth model can accurately reproduce pressure history and arrival time of detonation front. However, the parameters in ignition and growth model are obtained through cylinder test, thus, it is limited to describe long-term (millisecond scale) phenomenon, such as combustion of explosive gases and aluminum particles.

To investigate the mechanism of combustion of aluminum particles, researches have conducted both experiment and theoretical analysis. Boiko and Poplavski [2002] studied the ignition of aluminum powders in shock waves, and measured the relationship between reaction rate and temperature. [Kuhl *et al.* (2003, 2010a,b)] proposed a model to calculate the reaction rate for the combustion of aluminum under shock waves. Based on these models, Kuhl *et al.* [2010a] investigated the explosion of aluminized explosive. However, the model proposed by Kuhl is too complicated. It also has other disadvantages such as negative internal energy, which is incompatible with common model for high explosive such as ignition and growth model. Thus, a simplified afterburning model is employed in our paper. The idea is using a reaction rate model to describe the combustion of aluminum particles.

Thus, heat will be released with the combustion of aluminum particles. The details will be introduced below.

There have been a lot of literatures on the employment of the afterburning model. Togashi *et al.* [2012] investigated the detonation and afterburning effects of AFX 757 and TNT–Al in a confined facility. The simulation agrees well with measurements. Zhou *et al.* [2015] studied the detonation of aluminized explosive using similar model and obtained good result.

Smooth particle hydrodynamics (SPH) is a mesh-free Lagrangian method. Due to its advantage in tracking moving interfaces and dealing with large deformations, it has been used to solve hydraulic problem, ballistics problems and so on, which is difficult for traditional finite element method and finite volume method (FVM). Liu and Liu [2003], Liu *et al.* [2003a–c] investigated the feasibility of using SPH to simulate explosion of high explosives, underwater explosion and shaped charge detonation. However, the models for detonation in those literatures are either JWL or JWL++, which is much less accurate compared with ignition and growth model. Therefore, in this paper, a SPH method incorporated with ignition and growth model and afterburning model is proposed for the simulation of aluminized explosives.



## 2. Theoretical Models

### 2.1. *Governing equations in SPH method*

The governing equations for hydrodynamics problems are Navier–Stokes equations, which are conservation of mass, momentum and energy, respectively, as follows Liu and Liu [2003]:

$$\frac{d\rho}{dt} = -\rho \frac{\partial \mathbf{v}^{\beta}}{\partial \mathbf{x}^{\beta}}, \tag{1}$$

$$\frac{d\mathbf{v}^{\alpha}}{dt} = \frac{1}{\rho} \frac{\partial \sigma^{\alpha\beta}}{\partial x^{\beta}}, \tag{2}$$

$$\frac{de}{dt} = \frac{\sigma^{\alpha\beta}}{\rho} \frac{\partial v^{\alpha}}{\partial x^{\beta}} + \dot{q}, \tag{3}$$

where $\rho$ is density, $p$ is pressure of particle, $e$ is specific internal energy, $v$ is velocity and $\sigma$ is total stress tensor, $\dot{q}$ is source item (chemical heat), $t$ is time. The source item $\dot{q}$ plays critical role in the transition of shock wave to detonation wave.

For simplification, viscous shear stress is not considered in the governing equations. After manipulation, the original governing equations can be expressed as follows [Liu and Liu (2003)]:

$$\frac{d\rho_i}{dt} = \rho_i \sum_{j=1}^{N} \frac{m_j}{\rho_j} \mathbf{v}_{ij}^{\beta} \frac{\partial W_{ij}}{\partial \mathbf{x}_i^{\beta}}, \tag{4}$$

$$\frac{d\mathbf{v}_i^\alpha}{dt} = -\sum_{j=1}^{N} m_j \left( \frac{\sigma_i^{\alpha\beta}}{\rho_i^2} + \frac{\sigma_j^{\alpha\beta}}{\rho_j^2} + \prod_{ij} \right) \frac{\partial W_{ij}}{\partial \mathbf{x}_i^\beta}, \tag{5}$$

$$\frac{de_i}{dt} = \frac{1}{2} \sum_{j=1}^{N} m_j \left( \frac{p_i}{\rho_i^2} + \frac{p_j}{\rho_j^2} + \prod_{ij} \right) \mathbf{v}_{ij}^\beta \frac{\partial W_{ij}}{\partial \mathbf{x}_i^\beta} + \dot{q}, \tag{6}$$

where $m_j$ is particle mass of particle $j$, $W_{ij}$ is smoothing function for particle pair $i$, $j$, $\Pi_{ij}$ is artificial viscosity.

### 2.2. *Ignition and growth model for detonation*

The ignition and growth model is proposed by Lee and Tarver [1980], Tarver and McGuire [2002]. Compared with JWL model and JWL++ model, ignition and growth model introduces two physical assumptions (pressure equilibrium and temperature equilibrium), so it is more complicated and accurate. It can accurately reproduce arrival time of detonation wave and pressure history. Ignition and growth model has been successfully applied to various high explosives, including TATB, LX-17 and polymer-bonded explosives such as PBX 9404, PBX 9501. Due to these advantages, ignition and growth model has been integrated in commercial software such as ANSYS LS-DYNA.

Ignition and growth model includes two standard JWL equations of state, one for solid explosive and the other for gaseous products. Both of the EoSs have the form:

$$p = Ae^{-R_1 V} + Be^{-R_2 V} + \frac{\omega C_V T}{V}, \tag{7}$$

where $p$ is pressure, $V$ is volume ratio, $T$ is temperature, $C_V$ is the average heat capacity and $A$, $B$, $R_1$, $R_2, \omega$ are parameters fitted based on experiment.

The speed of sound is given by

$$c^2 = -\frac{V^2}{\rho_0} \frac{dp}{dV}, \tag{8}$$

where $p$ is pressure of solid explosive or explosive products.

Two assumptions are introduced in ignition and growth model, which are pressure equilibrium and temperature equilibrium. In the initial ignition and growth model, there is only pressure equilibrium. Afterwards, temperature equilibrium is introduced in the model as a standard approach for closure.

The reaction rate equation is:

$$\frac{d\lambda}{dt} = \lambda_1 + \lambda_2 + \lambda_3, \tag{9a}$$

$$\begin{cases} \lambda_1 = I\,(1-\lambda)^b \left( \dfrac{\rho}{\rho_0} - 1 - a \right)^x, & 0 < \lambda \le \lambda_{ig\,\max}, \\ \lambda_2 = G_1\,(1-\lambda)^c\,\lambda^d p^y, & 0 < \lambda \le \lambda_{G1\,\max}, \\ \lambda_3 = G_2\,(1-\lambda)^e\,\lambda^g p^z, & \lambda_{G2\,\min} \le \lambda < 1, \end{cases} \tag{9b}$$

where $I$, $a$, $b$, $x$, $c$, $d$, $y$, $e$, $g$, $z$, $G_1$, $G_2$, $\lambda_{ig\max}$ , $\lambda_{G1\max}$ and $\lambda_{G2\min}$ are rate constants, $\rho$ is the current density.

In the implementation of ignition and growth model, the status of reaction can be described by $\lambda$, ranging from 0 to 1.0 represents solid explosive, while 1 represents gaseous products. The number between 0 and 1 represents mixing status.

### 2.3. *Afterburning model for combustion of aluminum particles*

Afterburning model is common in the simulation of combustion. Miller [1995] proposed the idea to combine ignition and growth model with afterburning model. Ignition and growth model is used to describe the detonation of high explosive, while the afterburning model is used to describe the combustion of explosive gases or aluminum particles. Kuhl *et al.* [2003] proposed a different idea, which introduces temperature in their afterburning model. Thermodynamics code Cheetah is used to calculate the constituent of explosive gases. In addition, the specific internal energy of components of explosive gases is set to be negative at the beginning of the simulation, which is incompatible with ignition and growth model. The model has been used to study various explosives such as $SDF_1$ (an aluminized explosive, consisting of 45% $C_4H_8N_8O_8$, 35% Al, 20% $C_4H_6$), $SDF_2$ (a polyethylene-based fuel, consisting of 17% $C_5H_8N_4O_{12}$, 17% Al, 66% $C_4H_6$). The drawback is that it is quite complicated and requires Cheetah to obtain extra information (constituent of explosive gases) needed for the subsequent simulation.

The model proposed by Miller [1995] is employed in this paper. The EoS for the explosive gases is modified to the form [Togashi *et al.* (2010, 2012); Zhou *et al.* (2015); Miller (1995)]:

$$p = Ae^{-R_1V} + Be^{-R_2V} + \frac{\omega(C_VT + \alpha Q)}{V} \tag{10}$$

where $p$ is pressure, $V$ is volume ratio, and $A$, $B$, $R_1$, $R_2$, $w$ are parameters fitted according to experiment, $Q$ is the energy generated in the combustion of aluminum particles, $\alpha$ represents the process of combustion [Togashi *et al.* (2010)]:

$$\frac{d\alpha}{dt} = a(1-\alpha)^{1/2}\left(\frac{p}{p_0}\right)^{1/6}, \tag{11}$$

where $a$ is parameter fitted according to experiment, $p_0$ is atmospheric pressure. $a$ is set to be 1950 in all simulation of aluminized explosive.

## 3. Numerical Models

### 3.1. *Validation of ignition and growth model*

PBX 9501 is a widely used HMX-based plastic bonded explosive, which consists of 95% HMX, 2.5% Estane binder and 2.5% BDNPA/F. To validate the ignition and growth model, a 1D PBX 9501 model is proposed. The model is 0.02 m in length. The explosive bar is detonated using shock impact, as shown in Fig. 1.

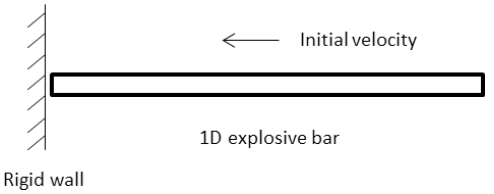


Fig. 1. 1D model of PBX 9501 bar.

Table 1. Parameters of JWL EoSs for solid explosive and gaseous products of PBX 9501.

| | $\rho_0$ (kg/m$^3$) | $A$ (GPa) | $B$ (GPa) | $R_1$ | $R_2$ | $\omega$ | $C_V$ (J/(kg·K)) |
|---|---|---|---|---|---|---|---|
| Solid PBX 9501 | 1,835 | 732000.00 | −5.2654 | 14.1 | 1.41 | 0.8867 | $2.7806 \times 10^6$ |
| Gaseous products of PBX 9501 | 1,835 | 1668.9 | 59.69 | 5.9 | 2.1 | 0.45 | $1.0 \times 10^6$ |

Table 2. Reaction rate parameters of PBX 9501.

| Reaction rate parameters of PBX 9501 | |
|---|---|
| $I$ | $1.4 \times 10^{17}\,\mathrm{s}^{-1}$ |
| $a$ | 0.0 |
| $b$ | 0.667 |
| $x$ | 20.0 |
| $c$ | 0.667 |
| $d$ | 0.277 |
| $y$ | 2.0 |
| $e$ | 0.333 |
| $g$ | 1.0 |
| $z$ | 2.0 |
| $G_1$ | $130 \times 10^{-16}\,\mathrm{Pa}^{-y}\,\mathrm{s}^{-1}$ |
| $G_2$ | $400 \times 10^{-16}\,\mathrm{Pa}^{-z}\,\mathrm{s}^{-1}$ |
| $\lambda_{ig\max}$ | 0.3 |
| $\lambda_{G1\max}$ | 0.5 |
| $\lambda_{G2\max}$ | 0.5 |

The model consists of 4,000 particles. The particles are evenly distributed and smoothing length of each particle is set to be 1.5 times distance between two neighboring particles.

The parameters of ignition and growth model are listed in Table 1 [Tarver *et al.* (2002)].

The parameters for reaction rate are listed in Table 2 [Tarver *et al.* (2002)].

The initial velocity of 1D explosive bar is set to be 480 m/s. The variation of shock wave and detonation wave is shown in Fig. 2.

The build-up effect in the propagation of shock wave is well presented in Fig. 2. With the release of chemical heat, the shock wave becomes increasingly stronger. At around 0.01 m, the shock wave transforms into sustainable detonation wave.

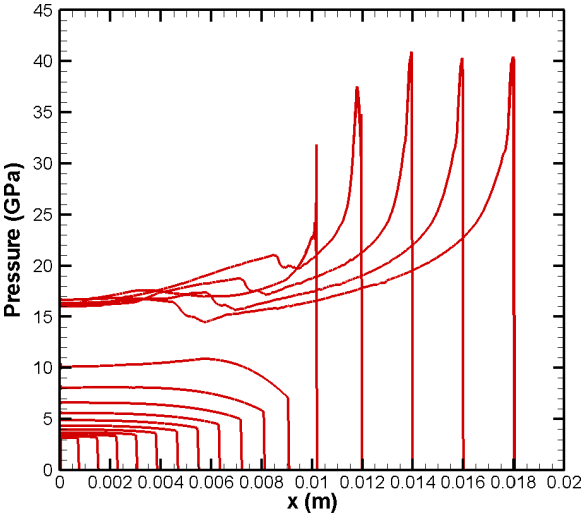


Fig. 2. Variation of shock wave. Each curve represents the distribution of pressure along the explosive bar at specific time.

The distribution of velocity, density and reaction along the explosive bar at 3.5 $\mu$s is shown in Fig. 3.

It can be seen from Fig. 3(c) that the reaction zone of high explosive is quite narrow. Solid explosive will promptly turn into explosive gases after detonation front passing through.

The comparison of simulation with FVM and experiment [Tarver *et al.* (2002)] is shown in Fig. 4. In the experiment, to record the pressure history at different locations, pressure gauges are embedded in the explosive bar, which are located, respectively, at 0, 5, 7, 9, 12 and 15 mm from detonation end.

It can be seen from Fig. 4 that SPH model incorporated with ignition and growth model can accurately reproduce the arrival time of detonation front. The pressure history at 7, 9, 12 and 15 mm calculated by SPH and FVM are quite similar, however, this is not the case for location 0 and 5 mm. This probably results from different boundary conditions in the two cases. The calculated peak pressure by SPH and FVM are also close to experiment. However, both simulation results are a little different from experiment. Due to the complexity of the detonation, numerical modeling is limited to describe all the details.

### 3.2. *Numerical model for simulation of aluminized explosive*

The aluminized explosive, we study is HMX–Al, which consists of 69% HMX, 15% Al, 7.5% GAP, 7.5% FomblinD and 1% isonate.

The 1D model is similar to the one described in Fig. 1. There are a total 2,000 particles (0.0292 m) in the model. The initial velocity of the aluminized explosive bar is set to be 1,000 m/s. Afterburning model is combined with ignition and growth

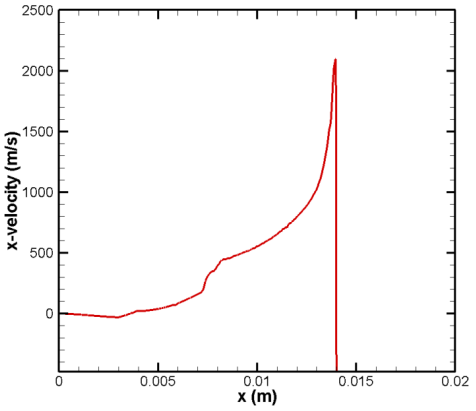


(a) $v_x$ along explosive bar

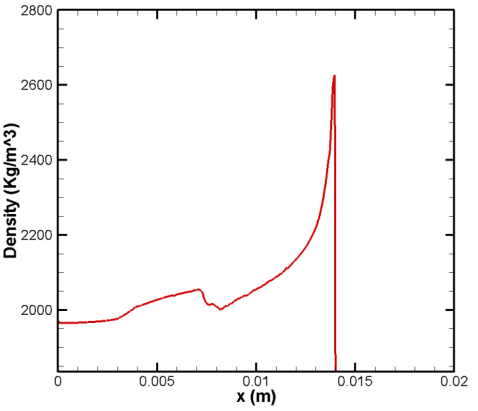


(b) Density along explosive bar

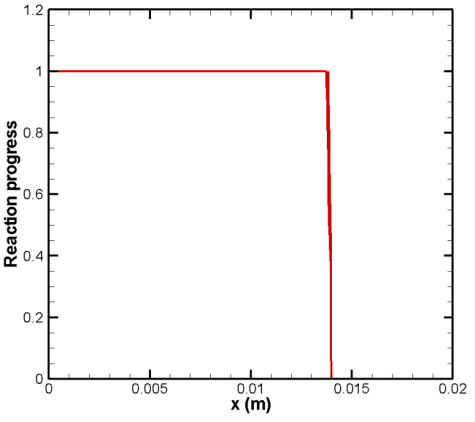


(c) Reaction progress along explosive bar

Fig. 3. Distribution of velocity, density and reaction progress along the explosive bar at 3.5 $\mu$s.

model for the simulation of aluminized explosive. Because combustion of aluminum particles is much slower than detonation, to simplify the model, it is assumed that combustion only happens to those particles that are in full gas state.

The evolution of pressure along the explosive bar is shown in Fig. 5.

The growth of shock wave can be clearly seen in Fig. 5. From left to right, as shock wave propagates in explosive, chemical energy is gradually released and the shock wave becomes increasingly stronger. Finally, the shock wave grows into self-sustainable detonation wave. The calculated peak pressure is close to Chapman–Jouguet pressure obtained in experiment [Manner *et al.* (2012)].

Compared to Fig. 2, it can be seen from Fig. 5 that peak pressure of aluminized explosive is reduced from 40 GPa to around 25 GPa. This is because the addition of aluminum particles reduces peak pressure in the initial stage of detonation (combustion of aluminum particle is much slower than detonation speed of HMX).

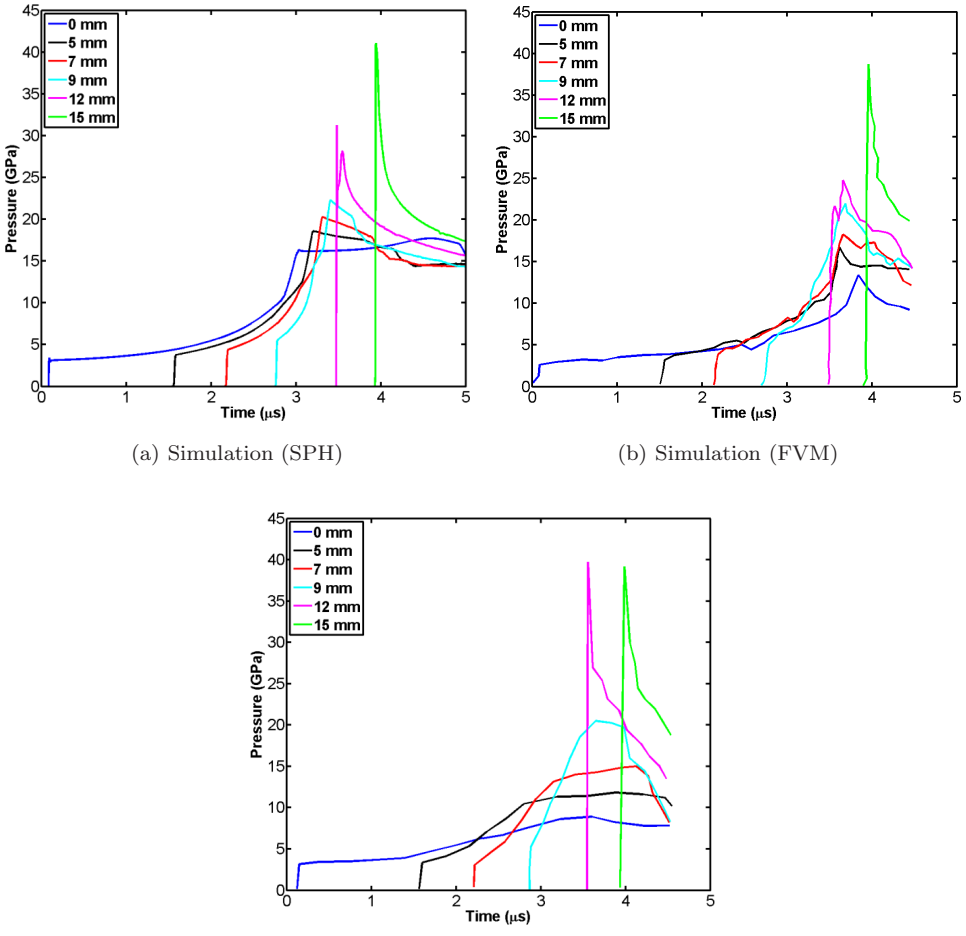


(a) Simulation (SPH)

(b) Simulation (FVM)

(c) Experiment

Fig. 4. Comparison of simulation with FVM and experiment.



However, aluminum particles are beneficial for the long-lasting heat release. The comparison of reaction progress of HMX and aluminum at 5 $\mu$s is shown in Fig. 6.

It can be seen that compared with high explosive, the reaction of aluminum particles is much slower.

The distribution of pressure, $x$-velocity and density is shown in Fig. 7.

The pressure history at different locations away from the left end of the bar is shown in Fig. 8. It can be seen that the pressure decreases rapidly with distance.

To investigate the influence of mass fraction of aluminum on performance of aluminized explosive, series of simulation is conducted, which includes different weight percent of aluminum, as shown in Table 3. Due to the scarcity of data, the weight percent of HMX, Al and other constituent are all assumed for simulation use.

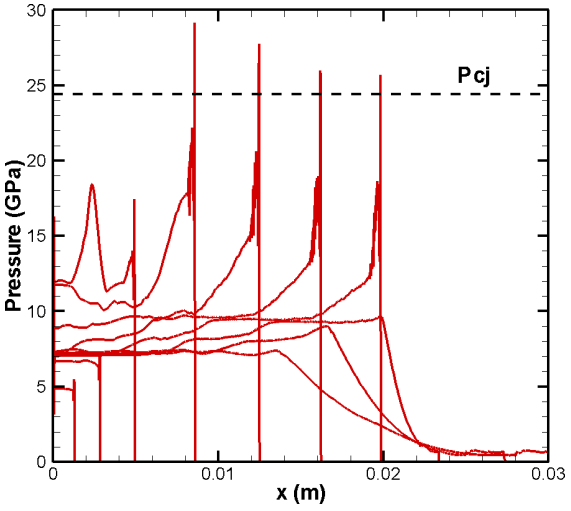


Fig. 5. Evolution of pressure along the aluminized explosive bar. Each curve represents distribution of pressure at specific time. From left to right, there are 10 curves in total and the time is from 1 $\mu$s to 10 $\mu$s.

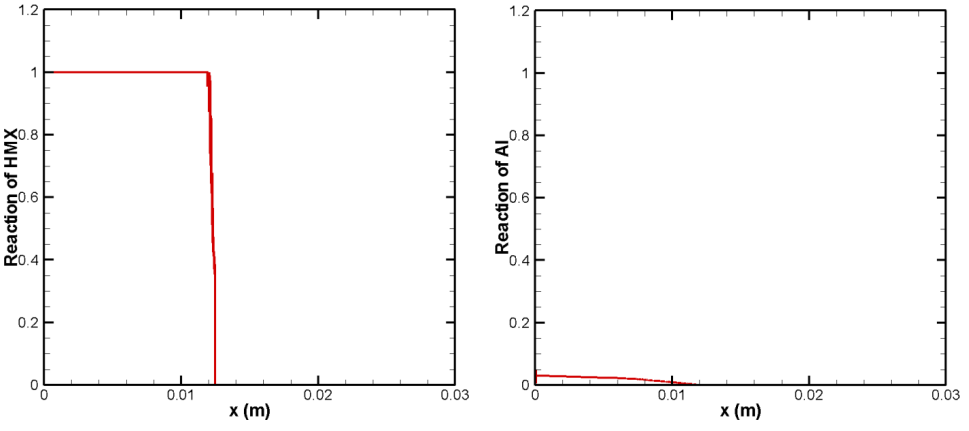


(a) Reaction of HMX (b) Reaction of aluminum particles

Fig. 6. Comparison of reaction progress of HMX and aluminum particles.

The influence of mass fraction of aluminum on pressure history at near-field and far-field is shown in Fig. 9.

The variation of pressure with mass fraction of aluminum is shown in Fig. 10. In Fig. 10(b), only the pressure of starting point of the smooth stage in Fig. 9(b) is extracted.

It can be seen from Fig. 10(a) that with the increase of aluminum, the peak pressure at near-field is reduced, which agrees with the analysis above. However,

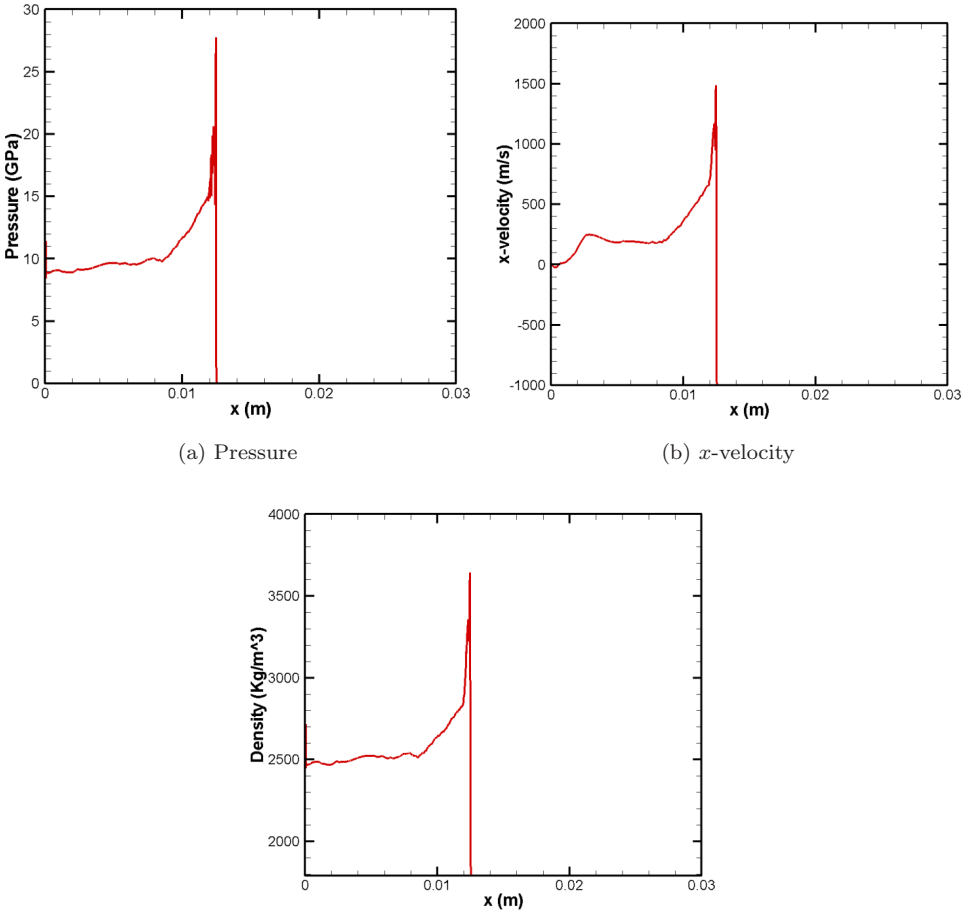


(a) Pressure

(b) $x$-velocity

(c) Density

Fig. 7. Distribution of pressure, $x$-velocity and density along the aluminized explosive bar.

for the far-field, the case is the opposite, as shown in Fig. 10(b). As time evolves, more aluminum starts to combust and increasing amount of heat is released, which enhances the pressure at far-field. Second-order curve and first-order curve is used to fit the near-field pressure and the far-field pressure. It can be seen from Fig. 10 that the fitted curves almost coincides with the original curves. The fitted formulas are as follows:

$$\begin{cases} p_{\text{near}} = -0.0133w^2 + 0.0215w + 29.8731, & 0 \le w \le 20, \\ p_{\text{far}} = 0.0179w + 0.3010, & 0 \le w \le 20. \end{cases} \tag{12}$$

The variation of impulse with mass fraction of aluminum is shown in Fig. 11. Second-order curve is used to fit the original curve. The fitted formula is as follows:

$$I_{\text{far}} = -26w^2 + 2291w + 22547, \quad 0 \le w \le 20 \tag{13}$$

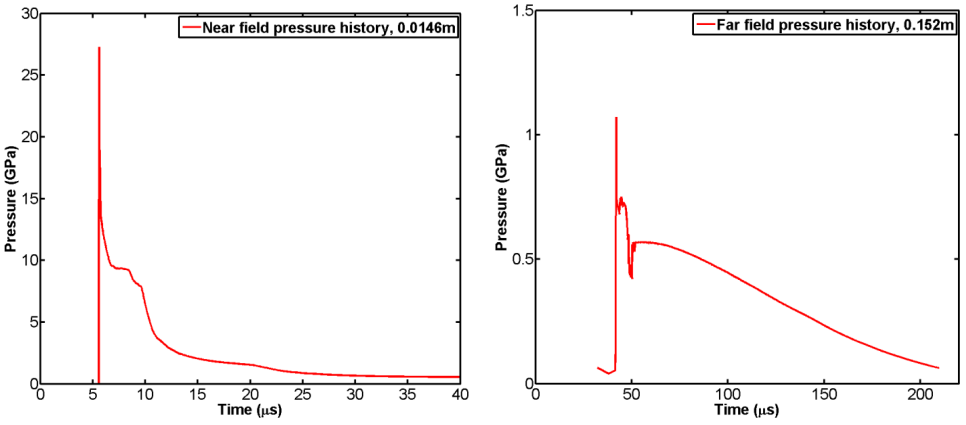


(a) Pressure history at near-field (b) Pressure history at far-field

Fig. 8. Pressure history of HMX–Al at near-field and far-field.

Table 3. Aluminized explosives with different mass fractions of aluminum.

| | HMX+0% Al | HMX + 5% Al | HMX + 10% Al | HMX + 15% Al | HMX + 20% Al |
|---|---|---|---|---|---|
| HMX (kg) | 1424.9 | 1363.4 | 1300.2 | 1234.9 | 1167.7 |
| Al (kg) | 0 | 86.83 | 176.28 | 268.47 | 363.52 |
| Others (kg) | 286.4 | 286.4 | 286.4 | 286.4 | 286.4 |

*Note*: All the simulations have the same configuration except the weight percent of aluminum.

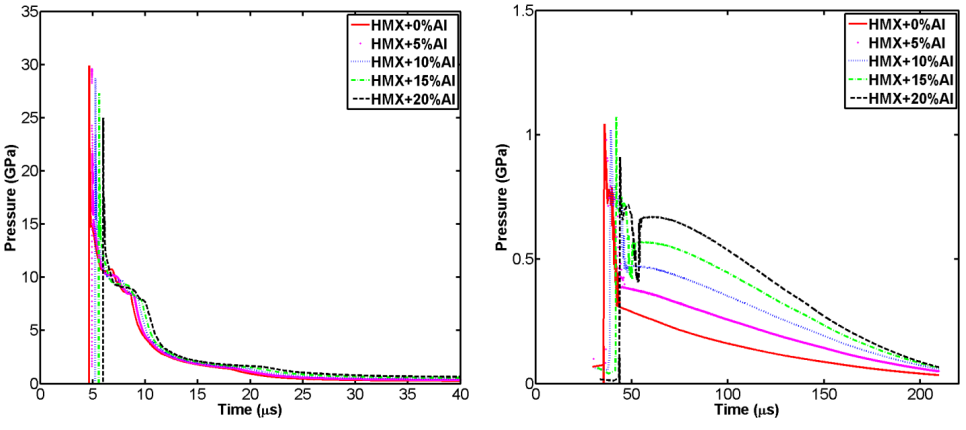


(a) 0.0146 m (b) 0.152 m

Fig. 9. Influence of mass fraction of aluminum on pressure history at near-field and far-field.

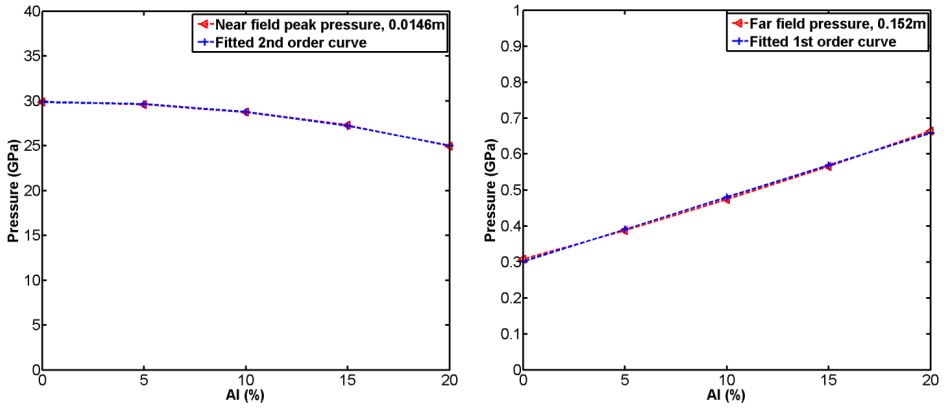


(a) Peak pressure in near-field (b) Pressure in far-field

Fig. 10. Variation of pressure with mass fraction of aluminum.

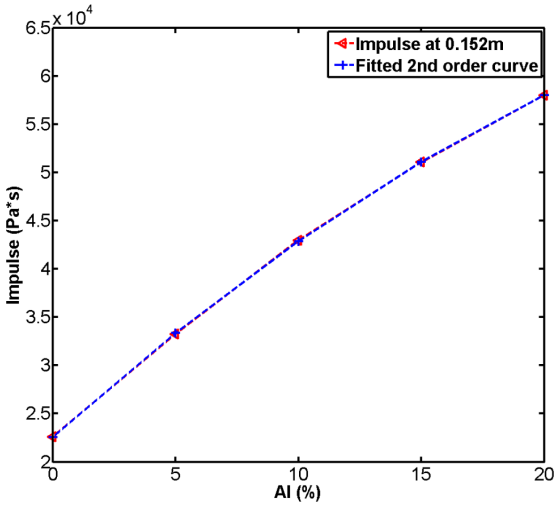


Fig. 11. Variation of impulse with mass fraction of aluminum.

## 4. Conclusion

SPH method is a mesh-free Lagrangian method. Compared with traditional finite element method and FVM, it has special advantages in tracking free surfaces and dealing with large deformation. In this paper, a SPH method that incorporates ignition and growth model and afterburning model has been proposed to study the detonation of aluminized explosives HMX-Al. The ignition and growth model is used to describe the detonation of HMX, while the afterburning model is used to describe combustion of aluminum particles. To verify the method, first, the ignition and growth model is validated. A simplified model of 1D PBX 9501 explosive bar is

developed. The calculated pressure history at different locations on the explosive bar is compared with that obtained through FVM and experiment and good agreement is observed. It is concluded that the SPH model is reliable and adequately accurate to simulate the detonation of high explosives.

Then, an afterburning model is integrated to the SPH codes to study aluminized explosives. The ignition and growth model is used to describe the detonation of high explosives, and the afterburning model is used to describe the combustion of aluminum particles. It is assumed that the combustion of aluminum particles only happens after the detonation of high explosive. To investigate the influence of mass fraction of aluminum on aluminized explosive, series of simulation are conducted. According to the simulation, with the increase of mass fraction of aluminum, the peak pressure in the near-field is reduced, however, in the far-field, due to the combustion of aluminum particles, the pressure increases.



## Acknowledgments

The work is mainly supported by the United States DoD (DTRA): Grant # HDTRA1-13-1-0025.

The authors would like to thank computing resource provided by Ohio Supercomputer Center.

## References

Bdzil, J. B. *et al.* [2002] "DSD front models: Nonideal explosive detonation in ANFO," *Proc. Int. 12th Symp.on Detoantion*, San Diego, CA, pp. 409–417.

Boiko, V. M. and Poplavski, S. V. [2002] "Self-ignition and ignition of aluminum powders in shock waves," *Shock Waves* **11**(4), 289–295.

Cook, M. A. *et al.* [1957] "Aluminized explosives," *J. Phys. Chem.* **61**(2), 189–196.

Cooper, P. W. [1996] *Explosives Engineering* (VCH, New York).

Cooper, P. W. and Kurowski, S. R. [1996] *Introduction to the Technology of Explosives* (VCH, New York).

Kuhl, A. L., Bell, J. B. and Beckner, J. B. [2010a] Heterogeneous continuum model of aluminum particle combustion in explosions, *Combust. Explos. Shock Waves* **46**(4), 433–448.

Kuhl, A. L., Bell, J. B. and Beckner, V. E. [2010b] "Gas-dynamic model of turbulent combustion in TNT explosions, *33rd Int. Combustion Symp.*, 1–6 August, Beijing, China.

Kuhl, A. L., Howard, M. and Fried, L. [2003] "Thermodynamic model of afterburning in explosions," *34th International ICT Conference*: *Energetic Materials*: *Reactions of Propellants, Explosives and Pyrotechnics*, 24–27 June 2003, Karlsruhe, Germany.

Lee, E. L. and Tarver, C. M. [1980] "Phenomenological model of shock initiation in heterogeneous explosives," *Phys. Fluids* **23**(12), 2362–2372.

Liu, G. R. and Liu, M. B. [2003] *Smoothed Particle Hydrodynamics:A Meshfree Particle Method* (World Scientific, Singapore).

Liu, M. B., Liu, G. R., Zong, Z. and Lam, K. Y. [2003a] "Computer simulation of high explosive explosion using smoothed particle hydrodynamics methodology," *Comput. Fluids* **32**(3), 305–322.

Liu, M. B., Liu, G. R., Lam, K. Y. and Zong, Z. [2003b] "Smoothed particle hydrodynamics for numerical simulation of underwater explosion," *Comput. Mech.* **30**(2),106–118.

Liu, M. B., Liu, G. R., Lam, K. Y. and Zong, Z. [2003c] "Meshfree particle simulation of the detonation process for high explosives in shaped charge unlined cavity configurations," *Shock Waves* **12**(6), 509–520.

Manner, V. M. *et al.* [2012] "The role of aluminum in the detonation and postdetonation expansion of selected cast HMX-based explosives," *Propell. Explos. Pyrotech.* **37**(2), 198–206.

Miller, P. J. [1995] "A reactive flow model with coupled reaction kinetics for detonation and combustion in non-ideal explosives," *Mat. Res. Soc. Proc.* **418**, 413–420.

Souers, P. C. *et al.* [2000] "JWL++: A simple reactive flow code package for detonation," *Propell. Explos. Pyrotech.* **25** (2), 54–58.

Tarver, C. M. [2005] "Ignition and growth modeling of LX-17 hockey puck experiments," *Propell. Explos. Pyrotech.* **30**(2), 109–117.

Tarver, C. M. *et al.* [2002] "Manganin gauge and reactive flow modeling study of the shock initiation of PBX 9501," *AIP Conf. Proc. Shock Compression of Condensed Matter-2001*, Vol. 620, AIP Press, Atlanta, CA, pp. 1043.

Tarver, C. M. and Chidester, S. M. [2009] "Modeling LX-17 detonation growth and decay using the ignition and growth model," *Shock Compression of Condensed Matter-2009, AIP Conference Proc.*, Vol. 1195, Nashville, USA, pp. 249–254.

Tarver, C. M. and Hallquist, J. O. [1981] "Modeling two-dimensional shock initiation and detonation-wave phenomena in PBX 9404 and LX-17," *Seventh Int. Symp. On Detonation,* 16–19 June 1981, Annapolis, MA, pp. 488–497.

Tarver, C. M. and McGuire, E. M. [2002] "Reactive flow modeling of the interaction of TATB detonation waves with inert materials," *Proc. 12th Int. Detonation Symp.*, San Diego, California, pp. 641–649.

Togashi, F. *et al.* [2002] "Numerical simulation of TNT–Al explosives in explosion chamber," *7th Int. Conf. on Computational Fluid Dynamics*, Big Island, Hawaii.

Togashi, F. *et al.* [2010] "Numerical simulation of long-duration blast wave evolution in confined facilities," *Shock Waves* **20**(5), 409–424.

Wackerle, J. *et al.* [1978] "A shock initiaison study of PBX-9404," *Shock* **1**(2), 5.

Wilkins, M. L., Squier, B. and Halperin, B. [1965] "Equation of state for detonation products of PBX 9404 and LX04-01," *Symp.* (*Int.*)*on Combustion*, Vol. 10, No. 1, pp. 769–778.

Zhou, Z. Q. *et al.* [2015] "A new method for determining the equation of state of aluminized explosive," *Chin. Phys. Lett.* **32**(1), 016401.